Inorg. Chem. **2002**, *41*, 4642–4652

A Spectrochemical Walk: Single-Site Perturbation within a Series of Six-Coordinate Ferrous Complexes†

Christian R. Goldsmith, Robert T. Jonas, Adam P. Cole, and T. Daniel P. Stack*

Department of Chemistry, Stanford University, California 94305

Received March 26, 2002

A series of ferrous complexes with the pentadentate ligand 2,6-(bis-(bis-2-pyridyl)methoxymethane)pyridine (PY5) was prepared and examined. PY5 binds ferrous iron in a square-pyramidal geometry, leaving a single coordination site accessible for complexation of a wide range of monodentate exogenous ligands: $[Fe^{II}(PY5)(X)]^{n+}$, X = MeOH, H_2O, MeCN, pyridine, Cl^-, OBz^-, N_3^-, MeO^-, PhO^-, and CN^-. The spin-states of these ferrous complexes are extremely sensitive to the nature of the single exogenous ligand; the spectroscopic and structural properties correlate with their high-spin (hs) or low-spin (ls) electronic ground state. Systematic metrical trends within six crystallographic structures clearly indicate a preferred conformational binding mode of the PY5 ligand. The relative binding affinities of the exogenous ligands in MeOH indicate that exogenous ligand charge is the primary determinant of the binding affinity; the $[Fe^{II}(PY5)]^{2+}$ unit preferentially binds anionic ligands over neutral ligands. At parity of charge, strong-field ligands are preferentially bound over weak-field ligands. In MeOH, the pK_a of the exogenously ligated MeOH in $[Fe(PY5)(MeOH)]^{2+}$ (9.1) limits the scope of exogenous ligands, as strongly basic ligands preferentially deprotonate $[Fe(PY5)(MeOH)]^{2+}$ to yield $[Fe(PY5)(OMe)]^{1+}$ rather than ligate to the ferrous center. Exogenous ligation by a strongly basic ligand, however, can be achieved in polar aprotic solvents.

Introduction

Ferrous iron demonstrates a remarkable ability to accommodate a diverse set of coordination geometries from four- to eight-coordinate, although the six-coordinate octahedral geometry is usually favored.[1] This binding plasticity is an important property in the bioinorganic chemistry of Fe(II), particularly in mononuclear non-heme oxidative enzymes. The ligand set and geometry in non-heme enzymes are much more varied than in heme-containing enzymes. Crystallographic and spectroscopic data of non-heme iron sites support both penta- and hexacoordination with nitrogen, oxygen, and sulfur donors derived from amino acid residues and exogenous ligands (Table 1).[2,3] This coordinative diversity increases the number of possible mechanisms for substrate and O_2 activation. Increased efforts to discern the relationship between structure and function in these mononuclear non-heme enzymes that activate O_2 have been made in recent years.[2−7] Similar studies on small molecule models have also been a valuable tool in the study of mononuclear non-heme iron enzymes.

Table 1. Mononuclear Non-Heme Iron Enzyme Active Site Ligands

enzyme[a]	geometry[b]	ox. state[b]	coordination ligands[b]	ref
3,4-PCD	trig. bipyramidal	Fe(III)	2N(His), 2O(Tyr), 1O(OH^-)	40, 41
BphC	sq. pyramidal	Fe(II)	2N(His), 1O(Glu), 2O(H_2O)	42, 43
SLO-1	octahedral	Fe(II)	3N(His), 1O(Ile−CO_2^-), 1O(Asn), 1O(H_2O)	44, 45
15-RLO	sq. pyramidal	Fe(II)	4N(His), 1O(Ile−CO_2^-)	46
PAH	octahedral	Fe(II)	2N(His), 1O(Glu), 3O(H_2O)	47
CAS	octahedral	Fe(II)	2N(His), 1O(Glu), 3O(H_2O)	48
IPNS	octahedral	Fe(II)	2N(His), 1O(Asp), 3O(H_2O)	49
SOD	trig. bipyramidal	Fe(II)	3N(His), 1O(Asp), 1O(H_2O)	50
SOR	sq. pyramidal	Fe(II)	4N(His), 1S(Cys)	51

[a] 3,4-PCD = protocatechuate 3,4-dioxygenase; BphC = 2,3-dihydroxybiphenyl 1,2-dioxygenase; SLO-1 = soybean lipoxygenase-1; SLO-3 = soybean lipoxygenase-3; 15-RLO = rabbit 15-lipoxygenase; PAH = human phenylalanine hydroxylase; CAS = clavaminic acid synthase; IPNS = microbial isopenicillin N-synthase; SOD = superoxide dismutase; SOR = superoxide reductase. [b] As determined in the crystallographic analysis.

Control of the geometric plasticity and ligand lability of Fe(II) sites can be achieved with conformationally restricted polydentate ligands, as found with porphyrins. These tet-

* To whom correspondence should be addressed. E-mail: stack@stanford.edu. Phone: (650) 725-8736. Fax: (650) 725-0259.

† Dedicated to Professor K. N. Raymond on the occasion of his 60th birthday.

(1) Cotton, F. A.; Wilkinson, G. *Advanced Inorganic Chemistry*, 5th ed.; Wiley-Interscience: New York, 1988.
(2) *Iron Metabolism. Inorganic Biochemistry and Regulatory Mechanisms*, 1st ed.; Ferreira, G. C.; Moura, J. J. G.; Franco, R., Eds.; Wiley: Weinheim, 1999.
(3) Que, L., Jr.; Ho, R. Y. N. *Chem. Rev.* **1996**, *96*, 2607−2624.
(4) Feig, A. L.; Lippard, S. J. *Chem. Rev.* **1994**, *94*, 759−805.
(5) Howard, J. D.; Rees, D. C. *Adv. Protein Chem.* **1991**, *42*, 199−280.
(6) Holm, R. H.; Kennepohl, P.; Solomon, E. I. *Chem. Rev.* **1996**, *96*, 2239−2314.
(7) Solomon, E. I. *Inorg. Chem.* **2001**, *40*, 3656−3669.

10.1021/ic025616z CCC: $22.00
Published on Web 07/30/2002

Scheme 1

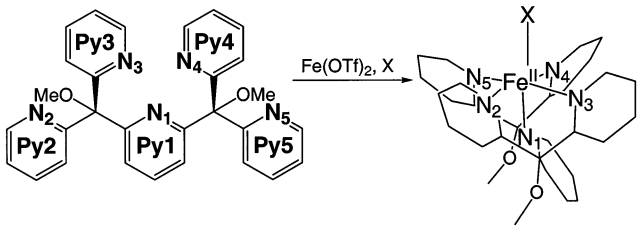

radentate ligands generally bind iron in a square-planar coordination, allowing variation of the axial ligand(s) to yield five- or six-coordinate complexes. This investigation concerns a pentadentate ligand with Fe(II) that imposes a square-pyramidal coordination geometry, thereby allowing facile variation of a single exogenous ligand. The number of noncyclic nitrogen ligands that enforce such a square-pyramidal conformation is limited to a few tetrapodal pentadentate ligands[8−12] and open chain penta-amines.[13]

In an effort to isolate structurally and functionally relevant analogues of lipoxygenase, a mononuclear non-heme iron enzyme, the ligand, 2,6-(bis-(bis-2-pyridyl)methoxymethane)-pyridine (PY5, Scheme 1), was designed and synthesized.[14,15] The five pyridine subunits of PY5 constitute a neutral five-coordinate metal binding cavity; complexation of a divalent metal results in a strongly Lewis acidic metal center. Reactions of PY5 with $Fe^{II}(OTf)_2$ ($OTf^- =$ triflate, $CF_3SO_3^-$) result exclusively in the isolation of six-coordinate complexes with the general cationic formula $[Fe^{II}(PY5)(X)]^{n+}$. The structural and spectroscopic properties of a series of Fe(II) complexes, $[Fe^{II}(PY5)(X)](OTf)_n$, with X = MeOH, H_2O, MeCN, pyridine, OBz^-, Cl^-, N_3^-, MeO^-, PhO^-, and CN^-, are presented. In addition, the relative binding affinities of these exogenous ligands to $[Fe^{II}(PY5)]^{2+}$ in MeOH highlight the importance of ligand charge over other electronic bonding features in determining the stability of a metal complex. In all cases, PY5 maintains a square-pyramidal ligation geometry with a single exogenous ligand, X, completing the metal coordination to generate a six-coordinate ferrous complex. An intriguing aspect of this work is that variation of X is sufficient to change the spin-state of the metal and thus the structural and electronic properties of the complex.

Results

Metal Complex Syntheses. The synthesis, characterization, and X-ray structure of 2,6-(bis-(bis-2-pyridyl)-methoxymethane)pyridine (PY5) have been described previously.[14,16] The Fe(II) complexes can be anaerobically synthesized in a variety of solvents from an equimolar ratio of PY5 and $Fe^{II}(OTf)_2$. The ligand accommodates a single metal ion in a six-coordinate octahedral conformation with the general formula $[Fe^{II}(PY5)(X)](OTf)_n$ ($n = 1$ or 2). The sixth coordination site is readily occupied by a coordinating solvent molecule, such as MeOH, H_2O, MeCN, or pyridine, to yield $[Fe(PY5)(solvent)](OTf)_2$. The H_2O complex is synthesized by mixing PY5 and $Fe^{II}(OTf)_2$ in nondried 2-propanol. The exogenous solvent ligand may be displaced with numerous anionic ligands, including chloride, methoxide, benzoate, azide, and cyanide, by addition of 1 equiv of their sodium or potassium salt (Scheme 2). The chloride complex [Fe(PY5)(Cl)](OTf) can also be synthesized by mixing PY5 with $Fe^{II}Cl_2$, followed by 1 equiv of Ag(OTf) to precipitate 1 equiv of Cl^- as AgCl(s).

Metal Complex Characterization. The following Fe(II) complexes, $[Fe(PY5)(MeOH)]^{2+}$, $[Fe(PY5)(H_2O)]^{2+}$, $[Fe(PY5)(MeCN)]^{2+}$, $[Fe(PY5)(pyridine)]^{2+}$, $[Fe(PY5)(OBz)]^{1+}$, $[Fe(PY5)(Cl)]^{1+}$, $[Fe(PY5)(N_3)]^{1+}$, $[Fe(PY5)(OMe)]^{1+}$, $[Fe(PY5)(OPh)]^{1+}$, and $[Fe(PY5)(CN)]^{1+}$, were isolated and characterized as their triflate salts by ^1H NMR spectroscopy, UV−vis absorption spectroscopy, mass spectroscopy, cyclic voltammetry, and solution magnetic susceptibility.[17]

A. Solution Structures. All of the examined $[Fe^{II}(PY5)(X)](OTf)_n$ complexes are stable upon exposure to air except [Fe(PY5)(OMe)](OTf) (in MeOH) and [Fe(PY5)(OPh)](OTf) (in acetone); both complexes undergo slow decomposition to free ligand and an insoluble iron product. Isolated solid samples of the other complexes retain their coordination when dried in vacuo at room temperature (RT).

^1H NMR spectroscopic characterization of the series of ferrous complexes at RT reveals both high-spin (hs) and low-spin (ls) complexes within the series (Table 2). The ^1H NMR spectra of $[Fe(PY5)(MeOH)]^{2+}$, $[Fe(PY5)(H_2O)]^{2+}$, $[Fe(PY5)(N_3)]^{1+}$, $[Fe(PY5)(OBz)]^{1+}$, $[Fe(PY5)(Cl)]^{1+}$, $[Fe(PY5)(OMe)]^{1+}$, and $[Fe(PY5)(OPh)]^{1+}$ exhibit features of hs ferrous complexes, with paramagnetically shifted peaks in the range −12 to 65 ppm. Solution magnetic susceptibilities[17] are in agreement with those expected for hs complexes. For the complexes $[Fe(PY5)(MeCN)]^{2+}$, $[Fe(PY5)(pyridine)]^{2+}$, and $[Fe(PY5)(CN)]^{1+}$, diamagnetic ^1H NMR spectra are observed, consistent with their assignment as ls complexes. In solution, PY5 is presumed to ligate Fe(II) in the manner demonstrated in Scheme 1. The highly symmetric nature of the ^1H NMR spectra of these complexes suggests dynamic averaging on the NMR time scale; all the equatorial pyridine resonances (Scheme 1, Py_{2-5}) are structurally equivalent.

Cyclic voltammetric measurements of $[Fe^{II}(PY5)(X)]^{n+}$ complexes in MeOH, acetone, or MeCN (Table 2) reveal very positive oxidation potentials for all the complexes. The four complexes with ligated solvent (X = H_2O, MeOH, MeCN, pyridine) show irreversible oxidation peaks above 0.9 V versus SHE while five of the complexes with anionic axial ligands (X = Cl^-, OBz^-, MeO^-, PhO^-, CN^-) show

(8) Grohmann, A.; Knoch, F. *Inorg. Chem.* **1996**, *35*, 7932−7934.
(9) Tamagaki, S.; Kanamaru, Y.; Ueno, M.; Tagaki, W. *Bull. Chem. Soc. Jpn.* **1991**, *64*, 165−174.
(10) Takano, S.; Yano, Y.; Tagaki, W. *Chem. Lett.* **1981**, 1177−1180.
(11) Lubben, M.; Meetsma, A.; Wilkinson, E. C.; Feringa, B. L.; Que, L., Jr. *Angew. Chem., Int. Ed. Engl.* **1995**, *34*, 1512−1514.
(12) Bernal, I.; Jensen, I. M.; Jensen, K. B.; McKenzie, C. J.; Toftlund, H.; Tuchagues, J.-P. *J. Chem. Soc., Dalton Trans.* **1995**, 3667−3675.
(13) Guajardo, R. J.; Chavez, F.; Farinas, E. T.; Mascharak, P. K. *J. Am. Chem. Soc.* **1995**, *117*, 3883−3884.
(14) Jonas, R. T.; Stack, T. D. P. *J. Am. Chem. Soc.* **1997**, 8566−8567.
(15) deVries, M. E.; LaCrois, R. M.; Roelfes, G.; Kooijman, H.; Spek, A. L.; Hage, R.; Feringa, B. L. *Chem. Commun.* **1997**, 1549−1550.
(16) Goldsmith, C. R.; Jonas, R. T.; Stack, T. D. P. *J. Am. Chem. Soc.* **2002**, *124*, 83−96.
(17) Evans, D. F. *J. Chem. Soc.* **1959**, 2003−2005.

Scheme 2

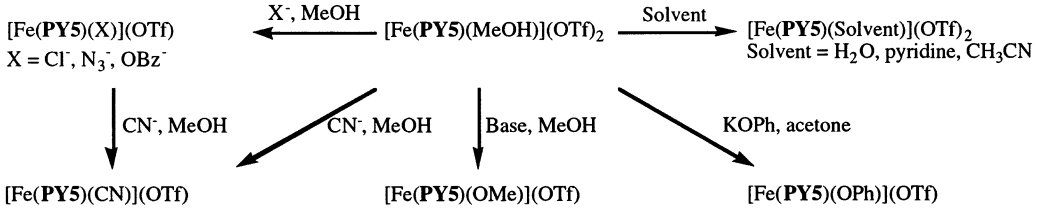

Table 2. Effective Magnetic Moments, ^{1}H NMR Resonance Ranges, and Redox Potentials of Ferrous Complexes[a]

complex	μ_{eff}[b] (μ_B)	spin-state	^{1}H NMR[d] range[c] (ppm)	$E_{1/2}$[d] (V)
$[Fe(PY5)(MeOH)]^{2+}$	4.7	hs	−11.3−57.0	0.930 (ΔE = 0.140 V)
$[Fe(PY5)(H_2O)]^{2+}$	4.9	hs	−11.8−58.0	1.360 (ΔE = 0.180 V)[e]
$[Fe(PY5)(Cl)]^{1+}$	5.1	hs	−11.2−64.1	0.990 (ΔE = 0.090 V)
$[Fe(PY5)(OBz)]^{1+}$	*g*	hs	−8.2−54.4	1.030 (ΔE = 0.160 V)
$[Fe(PY5)(OMe)]^{1+}$	4.7	hs	−10.8−60.1	0.760 (ΔE = 0.100 V)
$[Fe(PY5)(OPh)]^{1+}$	4.9	hs	−5.8−56.2	1.070 (ΔE = 0.090 V)[e]
$[Fe(PY5)(N_3)]^{1+}$	4.7	hs	−9.9−54.1	0.740 (irrev)
$[Fe(PY5)(MeCN)]^{2+}$	0	ls	4.08−9.97	1.150 (ΔE = 0.090 V)[f]
$[Fe(PY5)(pyridine)]^{2+}$	0	ls	4.68−13.38	1.180 (ΔE = 0.100 V)
$[Fe(PY5)(CN)]^{1+}$	0	ls	4.03−10.11	0.920 (ΔE = 0.090 V)

[a] Temperature = 292 K for solution measurements. [b] All measurements in acetone-d_6 except for $[Fe(PY5)(MeCN)]^{2+}$, which was measured in CD_3CN. [c] Shifts are reported in ppm from a TMS internal standard in acetone-d_6. [d] Redox potentials vs SHE. Referenced to the Fc/Fc^+ couple in MeOH (0.610 V)[34] except where noted. [e] Measured in acetone and referenced to the Fc/Fc^+ couple (0.700 V).[34] [f] Measured in MeCN and referenced to the Fc/Fc^+ couple (0.590 V).[34] [g] $[Fe(PY5)(OBz)]^{1+}$ was not soluble enough in acetone to acquire an accurate magnetic moment.

Table 3. UV−Vis Absorption Data of Ferrous Complexes

complex	solvent	λ_{max}[a] (ϵ[b])
$[Fe(PY5)(MeOH)]^{2+}$	MeOH	370 (1650), 785 (10), 865 (10)
$[Fe(PY5)(H_2O)]^{2+}$	2-propanol	355 (1580), 568 (20), 775 (20)
$[Fe(PY5)(Cl)]^{1+}$	MeOH	330(1590), 390 (1930), 860 (15)
$[Fe(PY5)(OBz)]^{1+}$	MeOH	330 (1630), 395 (1800)
$[Fe(PY5)(OPh)]^{1+}$	acetone	355 (1650), 428 (1530)
$[Fe(PY5)(N_3)]^{1+}$	MeOH	410 (2150), 810 (20)
$[Fe(PY5)(OMe)]^{1+}$	MeOH	340 (1300), 440 (1700), 715 (30)
$[Fe(PY5)(MeCN)]^{2+}$	MeCN	362 (6900), 384 (6900), 424 (5880), 554 (180)
$[Fe(PY5)(pyridine)]^{2+}$	pyridine	396 (4700), 440 (3000), 548 (190)
$[Fe(PY5)(CN)]^{1+}$	MeOH	372 (6700), 439 (8100)

[a] Absorption maxima reported in units of nm and measured to 1000 nm. [b] Extinction coefficients reported in units of M^{-1} cm^{-1}.

quasireversible cyclic voltammograms between 0.7 and 1.1 V versus SHE. $[Fe(PY5)(N_3)]^{1+}$ shows an irreversible oxidation peak at 0.740 V versus SHE. The ls complexes tend to exhibit oxidation potentials slightly higher than the hs complexes.

Differentiation of hs from ls ferrous complexes at RT is possible by simple visual inspection. Solutions of the seven hs complexes are varied shades of yellow and light orange, while solutions of the three ls complexes are deep orange to red. UV−vis absorption spectroscopy data corroborate the visual assignments (Table 3). All ten complexes show high energy transitions between 340 and 440 nm that are assigned as metal-to-ligand charge transfers (MLCT) between the Fe(II) center and the pyridine subunits of PY5. The maximum extinction coefficients for the MLCT absorptions of the hs complexes $[Fe(PY5)(MeOH)]^{2+}$, $[Fe(PY5)(H_2O)]^{2+}$, $[Fe(PY5)(Cl)]^{1+}$, $[Fe(PY5)(OMe)]^{1+}$, and $[Fe(PY5)(OPh)]^{1+}$ are between 1500 and 2200 M^{-1} cm^{-1} (Figure 1), much less intense than those of the ls complexes $[Fe(PY5)(MeCN)]^{2+}$, $[Fe(PY5)(pyridine)]^{2+}$, and $[Fe(PY5)(CN)]^{1+}$ with extinction coefficients in the range 5000−8000 M^{-1} cm^{-1} (Figure 2). The ls complexes moderately absorb near 550 nm. Higher

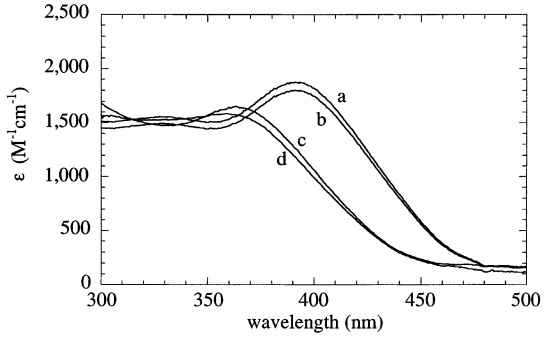

Figure 1. UV−vis spectra for complexes (a) $[Fe(PY5)(Cl)](OTf)$, (b) $[Fe(PY5)(OBz)](OTf)$, (c) $[Fe(PY5)(MeOH)](OTf)_2$, and (d) $[Fe(PY5)(H_2O)](OTf)_2$ at RT. All spectra were taken with ca. 5.5 mM samples in MeOH with the exception of $[Fe(PY5)(H_2O)](OTf)_2$, which was taken with a 2.5 mM sample in 2-propanol.

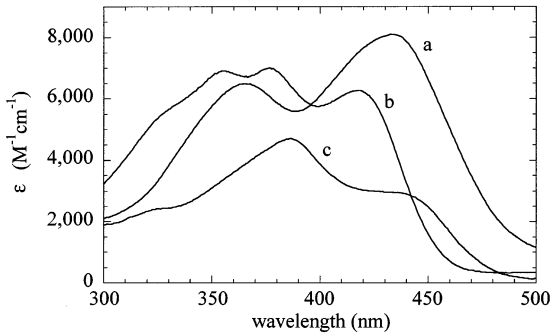

Figure 2. UV−vis spectra for low-spin complexes: (a) $[Fe(PY5)(CN)](OTf)$, (b) $[Fe(PY5)(MeCN)](OTf)_2$, and (c) $[Fe(PY5)(pyridine)](OTf)_2$ at RT. All spectra were taken of ca. 3.0 mM samples in MeOH with the exception of $[Fe(PY5)(MeCN)](OTf)_2$ which was taken in MeCN.

energy features below 300 nm are observed in the absorption spectra of all these complexes and likely result from metal-independent $\pi \rightarrow \pi^*$ transitions within PY5. The unbound ligand absorbs strongly ($\epsilon \sim 10\,000$ M^{-1} cm^{-1}) at 250 nm.

Table 4. Crystallographic Data of High-Spin Ferrous Complexes

	[Fe(PY5)(H_2O)]($OTf)_2$	[Fe(PY5)(Cl)](OTf)·(MeOH)	[Fe(PY5)(OBz)](OTf)
formula	$C_{31}H_{27}N_5O_9F_6S_2Fe$	$C_{62}H_{54}N_{10}O_{12}F_6S_2Fe_2$	$C_{37}H_{30}N_5O_7F_3SFe$
fw (g mol^{-1})	847.54	1491.88	857.6
cryst syst	triclinic	monoclinic	orthorhombic
space group	$P\bar{1}$ (No. 2)	$P2_1/c$ (No. 14)	*Pnma* (No. 69)
a (Å)	11.794(1)	18.396(1)	12.620(2)
b (Å)	12.291(2)	14.855(1)	14.484(2)
c (Å)	13.954(4)	23.090(1)	20.807(1)
α (deg)	80.68(2)	90.00	90.00
β (deg)	87.72(1)	102.262(1)	90.00
γ (deg)	62.49(1)	90.00	90.00
V ($Å^3$)	1769.1(6)	6166.4(1)	3803.1(8)
Z	2	4	4
μ_{calcd} (cm^{-1})	6.36	7.15	5.19
ρ_{calcd} (g cm^{-3})	1.591	1.610	1.50
crystal size (mm^3)	0.20 × 0.40 × 0.60	0.15 × 0.40 × 0.50	0.21 × 0.15 × 0.10
2θ range	10.0° < 2θ < 50.0°	10.0° < 2θ < 50.0°	3.23° < 2θ < 49.43°
reflns collected	6529	11 670	17 092
unique reflns	6200 (R_{int} = 0.188)	11 358 (R_{int} = 0.030)	3621 (R_{int} = 0.084)
reflns with ($F_o^2 > 3.00\sigma(F_o^2)$)	3510	6702	3354
no. params	487	865	299
reflns/params ratio	7.21	7.75	11.2
p-factor	0.010	0.006	0.010
R^a	0.078	0.051	0.049
$R_w{}^a$	0.071	0.057	0.123

[a] $R = \sum||F_o| - |F_c||/\sum|F_o|$; $R_w = [\sum w(|F_o| - |F_c|)^2/\sum wF_o^2]^{1/2}$, where $w = 4F_o^2/\sigma^2(F_o^2)$; $\sigma^2(F_o^2) = S^2(C + R^2B) + (pF_o^2)^2/(Lp)^2$ with S = scan rate, C = total integrated peak count, R = ratio of scan time to background counting time, B = total background count, Lp = Lorentz polarization factor, and p = p-factor.

Mass spectroscopy data for the complexes reveal limited information about their structures. Most of the complexes lose their exogenous ligand before detection, such that the typical parent ion peak is consistent with $[Fe(PY5)](OTf)^{1+}$. For the four complexes with neutral exogenous ligands (H_2O, MeOH, MeCN, pyridine), only the spectrum for [Fe(PY5)-(H_2O)]$(OTf)_2$ shows any evidence for retention of the axial ligand, with a peak assigned to $[Fe(PY5)(H_2O)](OTf)^{1+}$ at 698.0. A $[Fe(PY5)(X)]^{1+}$ parent ion peak is observed in the spectra of [Fe(PY5)(Cl)](OTf), [Fe(PY5)(OMe)](OTf), and [Fe(PY5)(CN)](OTf), as well as a less intense $[Fe(PY5)](OTf)^{1+}$ peak.

B. Solid State Structures. The X-ray structures of five cationic species are reported here, all of which contain triflate counteranions: $[Fe(PY5)(H_2O)]^{2+}$, $[Fe(PY5)(pyridine)]^{2+}$, $[Fe(PY5)(OBz)]^{1+}$, $[Fe(PY5)(Cl)]^{1+}$, and $[Fe(PY5)(CN)]^{1+}$. Structures of $[Fe(PY5)(MeOH)](OTf)_2$[14,16] and [Fe(PY5)-(MeCN)]$(ClO_4)_2$[15] have been previously reported, and their metrical parameters will be used in comparisons. Structural and refinement data for the four hs and two ls complexes, as assessed by solution magnetic susceptibility at 298 K (vide supra), are summarized in Tables 4 and 5, respectively. The atom labeling schemes for the cations of all complexes are congruent in order to facilitate comparisons of structural parameters. The Fe(II) center in each complex is coordinated in a square-pyramidal geometry by PY5, and a distorted six-coordinate octahedral environment is achieved with binding of an exogenous anion or solvent molecule. For the purpose of discussion, an equatorial plane (Pl_{eq}) is defined by the least-squares-plane of the four nitrogen atoms N_{2-5} in their respective pyridine subunits Py_{2-5} (Scheme 1). The axial positions are occupied by the nitrogen atom (N_1) of the axial pyridine subunit (Py_1) and the heteroatom of the exogenous ligand. The centroid of each pyridine subunit (Py_n) is denoted as cPy_n. The centroids of the pyridine subunits and the quarternary carbons that link them (C_{quat}) are used to describe the angles between adjacent subunits.

Table 5. Crystallographic Data of Low-Spin Ferrous Complexes

	[Fe(PY5)(pyridine)]-$(OTf)_2$·(pyridine)	[Fe(PY5)(CN)]-(OTf)·(MeOH)
formula	$C_{41}H_{35}N_7O_8F_6S_2Fe$	$C_{32}H_{29}N_6O_6F_3SFe$
fw (g mol^{-1})	987.73	738.52
cryst syst	triclinic	triclinic
space group	$P\bar{1}$ (No. 2)	$P\bar{1}$ (No. 2)
a (Å)	10.058(4)	10.5306(4)
b (Å)	12.368(2)	12.6061(6)
c (Å)	16.847(4)	12.9532(6)
α (deg)	86.32(2)	76.544(4)
β (deg)	79.85(3)	88.724(3)
γ (deg)	89.54(3)	67.513(3)
V ($Å^3$)	2058.8(9)	1540.9(1)
Z	2	2
μ_{calcd} (cm^{-1})	5.60	6.30
ρ_{calcd} (g cm^{-3})	1.593	1.592
cryst size (mm^3)	0.25 × 0.40 × 0.50	0.15 × 0.50 × 0.50
2θ range	8.0° < 2θ < 46.8°	10.0° < 2θ < 50.0°
reflns collected	5346	5676
unique reflns	5006 (R_{int} = 0.083)	5408 (R_{int} = 0.014)
reflections with ($F_o^2 > 3.00\sigma(F_o^2)$)	3037	4728
no. params	586	442
reflns/params ratio	5.18	10.70
p-factor	0.010	0.011
R^a	0.061	0.042
$R_w{}^a$	0.067	0.057

[a] $R = \sum||F_o| - |F_c||/\sum|F_o|$; $R_w = [\sum w(|F_o| - |F_c|)^2/\sum wF_o^2]^{1/2}$, where $w = 4F_o^2/\sigma^2(F_o^2)$; $\sigma^2(F_o^2) = S^2(C + R^2B) + (pF_o^2)^2/(Lp)^2$ with S = scan rate, C = total integrated peak count, R = ratio of scan time to background counting time, B = total background count, Lp = Lorentz polarization factor, and p = p-factor.

The asymmetric unit of [Fe(PY5)(OBz)](OTf) contains half of the ferrous cation $[Fe(PY5)(OBz)]^{1+}$ as the complex resides on a crystallographic mirror plane. To facilitate comparison with the other structures, the nitrogens in the

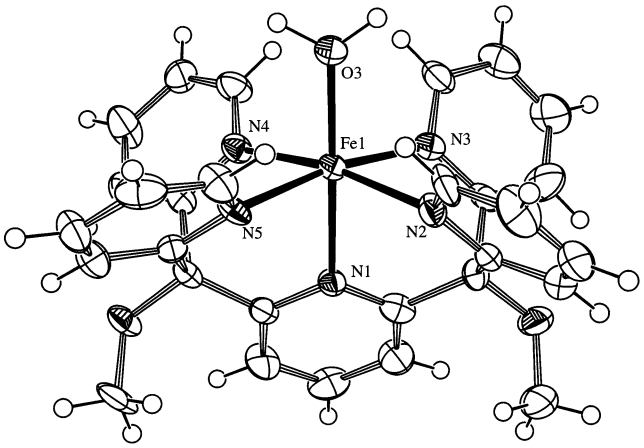

Figure 3. ORTEP representation of the crystal structure of $[Fe^{II}(PY5)(H_2O)]^{2+}$. Ellipsoids drawn at the 50% probability level.

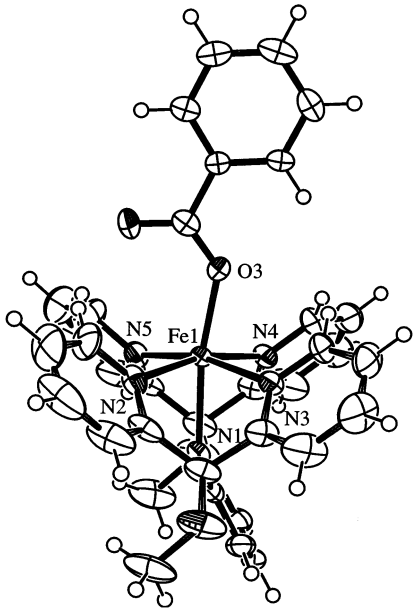

Figure 4. ORTEP representation of the crystal structure of $[Fe^{II}(PY5)(OBz)]^{1+}$. Ellipsoids drawn at the 50% probability level.

coordination sphere are appropriately designated N_{1-5}. The asymmetric unit of [Fe(PY5)(Cl)](OTf) contains two independent $[Fe(PY5)(Cl)]^{1+}$ cations (units A and B). The axial N_6 in the structure of unit B is congruent with N_1 in the structure of unit A. Likewise, the equatorial N_{7-10} in the structure of unit B are congruent with N_{2-5} in the structure of unit A. To facilitate comparison with the other structures, unit B will be treated as an independent structure with its coordination sphere nitrogens designated N_{1-5}. Full crystallographic reports with the original atomic labeling scheme for each complex are provided.[18]

All hs cations and $[Fe(PY5)(CN)]^{1+}$ share the distinctive PY5 binding motif previously reported.[14−16] The overall coordination is conserved throughout these five new stuctures. An ORTEP representation of $[Fe(PY5)(H_2O)]^{2+}$ is shown in Figure 3, while an orthogonal view of [Fe(PY5)(OBz)]$^{1+}$ is shown in Figure 4. ORTEP representations of the $[Fe(PY5)(Cl)]^{1+}$ and $[Fe(PY5)(CN)]^{1+}$ structures are available.[18] Selected bond lengths and angles are provided in Tables 6 (for hs complexes) and 7 (for ls complexes). As in previously reported structures,[14−16] the plane of Py_1 tilts relative to the perpendicular of Pl_{eq}, and the two methoxymethyl groups are positioned between Py_2 and Py_1 and between Py_5 and Py_1. These distortions create the distinctive binding structure of PY5. The $cPy_2-C_{quat}-cPy_1$ and $cPy_5-C_{quat}-cPy_1$ angles widen from the 108° seen in the free ligand to values between 118° and 123°. The bond lengths of Fe−N_2 and Fe−N_5 contract relative to Fe−N_3 and Fe−N_4, correlating with the opposite positioning to the tilt of Py_1. Last, the Fe(II) ion is displaced above Pl_{eq}. The ligand distortions and coordination sphere perturbations for all cations are summarized in Table 8. The average value of the Fe(1)−N(1−5) bond lengths is consistent with the solution spin-state assignments for each Fe(II) metal center. The axial cyanide ligand in $[Fe(PY5)(CN)]^{1+}$ is slightly askew with an Fe(1)−C(30)−N(6) bond angle of 174.1°. The Fe(1)−C(30) bond length of 1.925(3) Å is consistent with other Fe(II)−CN complexes.[19,20]

Table 6. Selected Bond Lengths and Angles for High-Spin Complexes[a]

complex[b]	MeOH	H_2O	OBz	Cl, unit A	Cl, unit B
Fe1−N1	2.097(3)	2.131(7)	2.185(5)	2.198(5)	2.215(5)
Fe1−N2	2.152(3)	2.149(8)	2.183(4)	2.182(5)	2.192(5)
Fe1−N3	2.203(3)	2.207(8)	2.267(3)	2.272(5)	2.263(5)
Fe1−N4	2.217(3)	2.242(7)	2.267(3)	2.252(4)	2.247(5)
Fe1−N5	2.141(4)	2.171(7)	2.183(4)	2.173(5)	2.179(5)
Fe1−X (X = O, Cl)	2.040(3)	2.034(6)	2.012(4)	2.311(2)	2.320(2)
N2−Fe1−N3	83.2(1)	80.4(3)	81.9(1)	80.5(2)	80.4(2)
N4−Fe1−N5	82.1(1)	83.7(3)	81.9(1)	80.4(2)	80.8(2)
N2−Fe1−N5	97.7(1)	95.8(3)	97.3(2)	95.1(2)	94.0(2)
N3−Fe1−N4	95.7(1)	98.5(3)	95.7(2)	100.5(2)	101.4(2)
N2−Fe1−N4	170.5(1)	168.9(3)	166.4(1)	164.6(2)	163.3(2)
N3−Fe1−N5	171.9(1)	170.7(3)	166.4(1)	166.8(2)	167.1(2)

[a] Bond lengths are in angstroms, and bond angles are in degrees. Estimated standard deviations in the least-squares figure are given in parentheses. [b] Complex names are abbreviated to the exogenous axial ligand for clarity.

Table 7. Selected Bond Lengths and Angles for Low-Spin Complexes[a]

[Fe(PY5)(pyridine)](OTf)$_2$		[Fe(PY5)(CN)](OTf)	
Fe1−N1	1.987(8)	Fe1−N1	1.980(2)
Fe1−N2	2.012(8)	Fe1−N2	2.000(2)
Fe1−N3	1.996(8)	Fe1−N3	2.068(2)
Fe1−N4	2.060(8)	Fe1−N4	2.043(2)
Fe1−N5	1.999(8)	Fe1−N5	2.003(2)
Fe1−N6	1.992(8)	Fe1−C30	1.925(3)
		C30−N6	1.159(4)
N2−Fe1−N3	85.0(3)	N2−Fe1−N3	82.7(1)
N4−Fe1−N5	84.0(3)	N4−Fe1−N5	84.9(1)
N2−Fe1−N5	96.3(3)	N2−Fe1−N5	97.5(1)
N3−Fe1−N4	94.6(3)	N3−Fe1−N4	94.9(1)
N2−Fe1−N4	178.9(3)	N2−Fe1−N4	177.6(1)
N3−Fe1−N5	175.5(3)	N3−Fe1−N5	176.2(1)
		Fe1−C30−N6	174.1(3)

[a] Bond lengths are in angstroms, and bond angles are in degrees. Estimated standard deviations in the least-squares figure are given in parentheses.

(18) See Supporting Information.

(19) Hsu, H. F.; Koch, S. A.; Popescu, C. V.; Münck, E. *J. Am. Chem. Soc.* **1997**, *119*, 8371−8372.
(20) Rauchfuss, T. B.; Contakes, S. M.; Hsu, S. C. N.; Reynolds, M. A.; Wilson, S. R. *J. Am. Chem. Soc.* **2001**, *123*, 6933−6934.

Table 8. Coordination Environment Structural Data for Ferrous Complexes

complex	spin-state[a]	N(1)[b]	av N(2,5)[b]	av N(3,4)[b]	av N(1−5)[b]	N(1) tilt[c]	Fe displ[d]	$cPy_2-C_{quat}-cPy_1$[e]	$cPy_5-C_{quat}-cPy_1$[e]
$[Fe(PY5)(Cl)]^{1+}$, unit B	hs	2.215	2.186	2.255	2.22	31.0	+0.286	119.5	120.8
$[Fe(PY5)(Cl)]^{1+}$, unit A	hs	2.198	2.178	2.262	2.22	28.9	+0.276	121.0	122.1
$[Fe(PY5)(OBz)]^{1+}$	hs	2.183	2.185	2.267	2.22	27.6	+0.264	122.9	122.9
$[Fe(PY5)(H_2O)]^{2+}$	hs	2.131	2.160	2.225	2.18	25.2	+0.195	118.9	123.3
$[Fe(PY5)(MeOH)]^{2+}$	hs	2.097	2.147	2.210	2.16	19.4	+0.167	121.4	121.6
$[Fe(PY5)(CN)]^{1+}$	ls	1.980	2.002	2.056	2.02	15.7	+0.055	121.6	118.0
$[Fe(PY5)(pyridine)]^{2+}$	ls	1.987	2.006	2.028	2.01	10.9	+0.049	117.0	112.6

[a] At RT as assessed by ^1H NMR. [b] Bond distances from Fe reported in units of angstroms. [c] Tilt in degrees of the axial pyridine ligand from the perpendicular of the least squares equatorial plane N(2−5). [d] Displacement of the Fe(II) ion from the equatorial plane N(2−5) in Å. [e] Measured in degrees, using the centroids of Py_1, Py_2, and Py_5. Bond angles are ∼108° in free PY5.

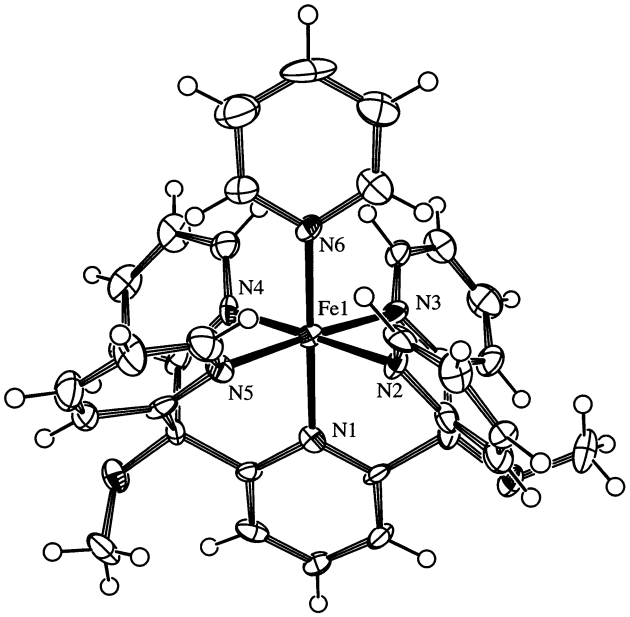

Figure 5. ORTEP representation of the crystal structure of $[Fe^{II}(PY5)(pyridine)]^{2+}$. Ellipsoids drawn at the 50% probability level. Note the unusual positioning of the methoxy group to the right.

The conformation of the PY5 ligand in $[Fe(PY5)(pyridine)](OTf)_2$ (Figure 5) slightly differs from that of the other structurally characterized complexes. Py_1 tilts to a lesser degree from the perpendicular of Pl_{eq} at 10.9°, and only one of the two methoxy groups is positioned analogously to the other structures. The second methoxy group is positioned upward into the cleft between Py_2 and Py_3 in a similar manner as found in the structure of free PY5.[16] As a consequence, the $cPy_2-C_{quat}-cPy_3$ angle of 113° is most similar to the $cPy_5-C_{quat}-cPy_1$ angle of 117°, as both reflect the accommodation of the methoxy group between two pyridine subunits. The other four $cPy-C_{quat}-cPy$ angles are significantly less than the idealized 109° angle. Correlated with the lessened tilt of Py_1, the bond lengths of $Fe-N_2$ (2.012(8) Å) and $Fe-N_5$ (1.999(8) Å) do not contract relative to $Fe-N_3$ (1.996(8) Å) and $Fe-N_4$ (2.060(8) Å) as observed in the other ferrous complexes. The exogenous pyridine ligand is coordinated perpendicular to Pl_{eq}, such that the 2- and 6-position hydrogen atoms of the ring are positioned into the clefts of the pyridyl arms. The exogenous pyridine Fe(1)−N(6) bond length of 1.992 Å is shorter than the average Fe(1)−N(1−5) bond length of 2.010 Å for PY5. Together, the average Fe−N bond lengths of the six pyridine moieties (2.007 Å) are consistent with the solution assignment of a ls Fe(II) complex.

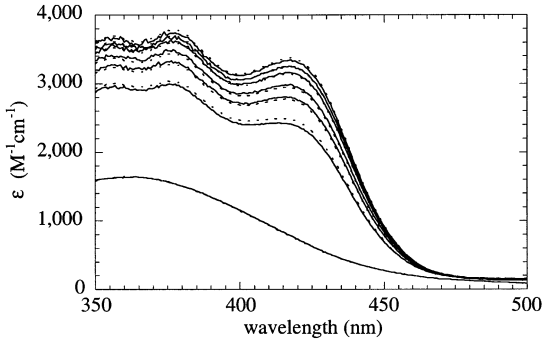

Figure 6. Titration of 1.6 mM $[Fe(PY5)(MeOH)]^{2+}$ in MeOH with pyridine. The solid lines represent the empirical data while the dashed lines represent the model fit. Amount of pyridine (equiv) added in order of increasing spectral intensity: 0, 3.3, 6.6, 10, 13, 20, 33. The end spectrum (33 equiv pyridine added) is ∼80% converted to $[Fe(PY5)(pyridine)]^{2+}$.[18]

Solution Chemistry. The axial ligands bound to $[Fe^{II}(PY5)]^{2+}$ are sufficiently labile enough to allow study of ligand exchange except for CN^-. $[Fe(PY5)(CN)]^{1+}$ remains unchanged over the course of hours in solutions with large excesses of pyridine, water, or Cl^- as assessed by optical spectroscopy. This lack of CN^- lability is similar to that observed for the ferrocyanide anion.[1] A series of spectrophotometric titrations in MeOH provides the relative binding affinities of MeCN, pyridine, Cl^-, OBz^-, N_3^-, and MeOH. Spectral deconvolution of the individual titrations over the 350−500 nm range clearly shows only two significant species. A representative titration of $[Fe(PY5)(MeOH)]^{2+}$ with pyridine to give $[Fe(PY5)(pyridine)]^{2+}$ is presented in Figure 6. The equilibrium constant for each two-species spectrophotometric titration was determined by a component analysis and a least-squares fit to a simple equilibrium model (eq 1).

$$[Fe^{II}(PY5)(X)]^{n+} + Y \rightleftharpoons [Fe^{II}(PY5)(Y)]^{n+} + X \quad (1)$$

In each case, projected spectra of the two pure species closely matched the experimentally determined spectra.[18] The binding affinities of MeCN and pyridine were measured relative to the binding affinity of MeOH, the weakest ligand examined, while the binding affinities of Cl^-, OBz^-, and N_3^- were measured relative to the binding affinity of pyridine. The relative equilibrium constants are summarized in Table 9. It should be noted that the solvent composition and the ionic strength of the solution change slightly during

Table 9. Relative Equilibrium Constants of Ferrous-PY5 Complexes in MeOH

ligand[a]	K(MeOH)[b]	K(pyr)[b]
MeOH	1	0.0003
MeCN	100(50)	
pyridine	3000(500)	1
OBz^-	5×10^6 [c]	2000(1000)
Cl^-	5×10^6 [c]	2000(1000)
N_3^-	2×10^8 [c]	80000(10000)

[a] This ligand (Y) was added as the titrant. [b] K(X) = ([Fe(PY5)(Y)] × [X])/([Fe(PY5)(X)] × [Y]) at 298 K. [c] Estimate based on value of K(MeOH) for pyridine.

each titration, and titration conditions were adjusted to minimize these changes. Ionic strength does have an effect on the observed equilibrium in experiments involving anionic titrants; the observed K_{eq} for the titration of $[Fe(PY5)(pyridine)]^{2+}$ to $[Fe(PY5)(Cl)]^{1+}$ nearly doubles when the system contains 0.06 M tetrabutylammonium perchlorate salt. The values presented here are only estimates for MeOH solution. The relative binding affinity for the studied ligands is MeOH < MeCN < pyridine $\ll Cl^- \sim OBz^- < N_3^- \ll CN^-$.

In MeOH, strong bases can deprotonate $[Fe(PY5)(MeOH)]^{2+}$ ($pK_a = 9.1 \pm 0.2$, MeOH)[16] to give $[Fe(PY5)(OMe)]^{1+}$, which is identifiable by its characteristic UV−vis spectrum (vide infra). When the base is a suitable ligand, the acid−base chemistry competes with ligand displacement. Phenolate (pK_a(phenol) = 14.3, MeOH), for instance, readily deprotonates $[Fe(PY5)(MeOH)]^{2+}$ in MeOH to form $[Fe(PY5)(OMe)]^{1+}$. However, when the reaction is run in acetone and monitored by UV−vis, another species is formed, tentatively assigned as $[Fe(PY5)(OPh)]^{1+}$. The use of an aprotic solvent medium appears to allow stronger bases to bind to Fe(II).

Discussion

Control of the coordination to Fe(II) is difficult because of the intrinsic coordinative ambivalence of the metal. Such control can be exerted through appropriate ligand design. To this end, the pentadentate ligand PY5 was synthesized and complexed to iron with a number of exogenous ligands. The apparent accessibility of the ligand periphery allows for a wide variety of substrates to bind in the sixth coordination site. Ten ferrous complexes $[Fe^{II}(PY5)(X)]^{n+}$, with X = MeOH, H_2O, MeCN, pyridine, Cl^-, MeO^-, OBz^-, N_3^-, phenolate, and CN^-, were examined. The exogenous ligands were chosen for their potential biochemical relevance, their coverage of the spectrochemical series, and the synthetic tractability of the resultant iron complexes.

The PY5 ligand was designed as an uncharged ligand in order to promote the formation of Lewis acidic metal centers. Cyclic voltammetric measurements on the ferrous complexes clearly show that the Fe(II) oxidation state is favored by PY5. The quasireversible redox potential of the $[Fe(PY5)(MeCN)]^{2+}$ complex in MeCN is 1.15 V versus SHE, a value similar to the high redox potentials measured for the hexapyridyl complexes $[Fe(bipy)_3]^{2+}$ (1.21 V vs SHE) and $[Fe(phen)_3]^{2+}$ (1.22 V vs SHE).[21,22] The high redox potentials of $[Fe^{II}(PY5)(X)]^{n+}$ complexes disfavor the formation of ferric complexes with PY5. Indeed, reactions of the ligand with Fe(III) salts in MeOH result in the isolation of $[Fe^{II}(PY5)(X)]^{n+}$ complexes, and only one $[Fe^{III}(PY5)(X)]^{n+}$ complex has been isolated to date.[16] The failure to isolate other $[Fe^{III}(PY5)(X)]^{n+}$ complexes is likely due to spontaneous reduction, as has been observed for other systems, presumably through oxidation of the solvent.[23,24] The redox potential of the ferrous complexes can be readily altered by the exogenous ligand. As observed in Table 2, anionic ligands tend to lower the redox potentials among the complexes examined in MeOH. The Coulombic attraction between an anionic ligand and a cationic metal center should better stabilize the ferric complex formed upon oxidation, thereby lowering the potential relative to a complex with a neutral exogenous ligand. In the case of high-spin (hs) complexes, the antibonding σ^* electron (the e_g set of d orbitals in an octahedral complex) may facilitate the loss of an electron relative to the low-spin (ls) complexes that lack electrons in this higher-energy orbital. Consequently, the redox potential is lowered with anionic and weak-field exogenous ligands.

The influence of the exogenous ligand on the metal center can also be examined with UV−vis absorption spectroscopy. Most complexes exhibit two metal-to-ligand charge transfer (MLCT) bands in the 300−500 nm range. The hs complexes' MLCT absorptions are weaker in intensity than those of the ls complexes, presumably as a result of weaker overlap between the metal π-bonding d orbitals and the ligand π^* orbitals. Broad absorption bands with small extinction coefficients ($\epsilon = 15-20\ M^{-1}\ cm^{-1}$) are observed for most hs complexes above 700 nm while moderately low intensity transitions are observed for most ls complexes near 550 nm. In $[Fe(PY5)(CN)]^{1+}$, this band may be obscured by the lower-energy MLCT band. Magnetic circular dichroism spectroscopy indicates that the two bands above 700 nm in $[Fe(PY5)(MeOH)]^{2+}$ are spin-allowed d→d transitions,[25] and it is likely that the bands seen above 700 nm for the other hs complexes are d→d transitions as well.

The exogenous ligand X in $[Fe^{II}(PY5)(X)]^{n+}$ controls the spin-state of the ferrous complex. The complex with the medium-field MeOH, $[Fe(PY5)(MeOH)]^{2+}$, has been shown to be a spin-transition species that is predominantly hs at room temperature (RT).[16] Stronger-field ligands such as MeCN, pyridine, or CN^- create ls complexes at RT. Comparing the ls $[Fe(PY5)(pyridine)]^{2+}$ to the hs $[Fe(pyridine)_6]^{2+}$ suggests that the five pyridine subunits of PY5 create a stronger ligand field than five independent pyridine ligands.[26] The field strength of PY5 on a per pyridine subunit

(21) Fukuzumi, S.; Kochi, J. K. *J. Am. Chem. Soc.* **1982**, *104*, 7599−7609.
(22) Wong, C. L.; Kochi, J. K. *J. Am. Chem. Soc.* **1979**, *101*, 5593−5603.
(23) Di Vaira, M.; Mani, F.; Stoppioni, P. *J. Chem. Soc., Dalton Trans.* **1997**, 1375−1379.
(24) Onggo, D.; Rae, A. D.; Goodwin, H. A. *Inorg. Chim. Acta* **1990**, *178*, 151−163.
(25) Pavel, E. G.; Kitajima, N.; Solomon, E. I. *J. Am. Chem. Soc.* **1998**, *120*, 3949−3962.
(26) Doedens, R. J.; Dahl, L. F. *J. Am. Chem. Soc.* **1966**, *88*, 4847−4855.

basis is most likely on par with 2,2′-bipyridine, a ligand that can also form spin-transition Fe(II) complexes.[27,28]

The ferrous structures of PY5 with six different monodentate ligands were determined by X-ray crystallography: $[Fe(PY5)(MeOH)]^{2+}$, $[Fe(PY5)(H_2O)]^{2+}$, $[Fe(PY5)(pyridine)]^{2+}$, $[Fe(PY5)(Cl)]^{1+}$, $[Fe(PY5)(OBz)]^{1+}$, and $[Fe(PY5)(CN)]^{1+}$. In each case, PY5 enforces the square pyramidal coordination configuration of Fe(II) with the exogenous ligand completing a six-coordinate metal geometry. Systematic structural distortions from an idealized octahedral coordination geometry are present in these structures. The Fe(1)−N(1) bond distance to PY5 is consistently the shortest of the five metal−pyridine bonds, and the Fe(II) is consistently displaced above the least-squares plane of N_{2-5}, Pl_{eq}. The most significant perturbations result from the skewing of Py_1 from the perpendicular of Pl_{eq} (Table 8). Correlated with the tilt of Py_1 is the positioning of the methoxy-methyl groups into the clefts between Py_2 and Py_1 and between Py_5 and Py_1. This positioning requires the $cPy_2-C_{quat}-cPy_1$ and $cPy_5-C_{quat}-cPy_1$ angles to be significantly opened relative to an idealized tetrahedral angle; the positioning of the methoxy-methyl group is noninnocent (Table 8).[29] As a consequence of the tilt of Py_1 and methoxy group positioning, a consistent distortion exists among the four equatorial Fe−N bond distances. The Fe(1)−N(2,5) bond lengths are considerably shorter than the Fe(1)−N(3,4) bond lengths.

The electronic properties and steric demands of the exogenous ligand modulate the magnitude of these perturbations. Strong-field ligands reduce the radius of the Fe(II) ion, thereby allowing the Fe(II) to sink further into Pl_{eq} and closer to Py_1. Py_1 tilts less as the ligand field strength increases, leading to smaller disparity in the equatorial bond distances. Using the average length of the five Fe−N bonds of PY5 as a measure of the Fe(II) ionic radius (Table 8), the iron size in these structures decreases along the series $[Fe(PY5)(Cl)]^{1+} \sim [Fe(PY5)(OBz)]^{1+} > [Fe(PY5)(H_2O)]^{2+} > [Fe(PY5)(MeOH)]^{2+} > [Fe(PY5)(pyridine)]^{2+} \sim [Fe(PY5)(CN)]^{1+}$, which is analogous to the ligand ordering in the spectrochemical series. These trends are also reflected in the RMS errors determined by structural overlays of the cations' coordination spheres.[18]

Study of the ligand exchange shows two significant trends. First, $[Fe^{II}(PY5)]^{2+}$ binds all anionic ligands examined preferentially over neutral ligands. This is readily explained by the Coulombic attraction between anionic ligands and the dicationic $[Fe^{II}(PY5)]^{2+}$ species. The binding affinities of anions relative to MeOH are sufficiently large to allow nearly stoichiometric formation of $[Fe^{II}(PY5)(X)]^{1+}$ ($X = Cl^-$, OBz^-, and N_3^-) in pure MeOH with ca. 1 mM concentration of $[Fe^{II}(PY5)]^{2+}$. Second, at parity of charge, the ligands that allow formation of ls Fe(II) complexes are bound preferentially to those that react to form hs Fe(II) complexes because of the increased ligand field stabilization energy of the ls complexes. The stabilization energy gained from going hs to ls is much less than that gained from binding of an anionic ligand. Consequently, weak-field anionic exogenous ligands are bound preferentially to strong-field neutral exogenous ligands.

The formation of $[Fe(PY5)(OPh)]^{1+}$ successfully occurs in acetone but not in MeOH, where the added phenolate instead leads to the complete formation of $[Fe(PY5)(OMe)]^{1+}$. This result is initially surprising given the superior acidity of PhOH (14.3)[30] compared to MeOH (19.6)[30] in MeOH. Even at millimolar concentrations of added PhO^-, the equilibrium concentration of PhO^- should be sufficiently larger than the equilibrium concentration of MeO^- in MeOH. This suggests that the binding affinity of MeO^- to $[Fe^{II}(PY5)]^{2+}$ is greater than that of PhO^-. Unfortunately, the binding affinity of MeO^- relative to MeOH is too large to be determined directly by a titration of MeO^- with $[Fe(PY5)(MeOH)]^{2+}$. Addition of competitive anions to solutions of $[Fe(PY5)(OMe)]^{1+}$ results in release of the Fe(II) from PY5 and concomitant bleaching of the solution. Instead, a thermodynamic analysis that uses the pK_a of $[Fe(PY5)(MeOH)]^{2+}$ in MeOH (9.1)[16] and the pK_a of MeOH estimates the relative binding affinity of MeO^- to be 3×10^{10} (eq 2). This binding constant is 2 orders of magnitude larger than those of the other anionic ligands with the exception of CN^- and may suggest some π-bonding in the Fe(II)−O bond similar to that observed in $[Fe^{III}(PY5)(OMe)]^{2+}$.[16] When PhO^- is added to $[Fe(PY5)(MeOH)]^{2+}$ in acetone, the competition with MeO^- is eliminated, allowing PhO^- to bind to $[Fe^{II}(PY5)]^{2+}$. These aprotic conditions provide a new route toward the synthesis of sub-site-differentiated $[Fe^{II}(PY5)(X)]^{n+}$ complexes.

$$[Fe(PY5)(MeOH)]^{2+} + MeO^- \rightleftharpoons [Fe(PY5)(OMe)]^{1+} + MeOH \quad (2)$$

Summary

The ligand PY5 was previously designed to stabilize high-spin Fe(II) complexes for the study of mononuclear non-heme iron enzymes. The structural analysis of a series of iron complexes shows the intrinsic property of PY5 to chelate Fe(II) in a square-pyramidal coordination geometry. The ligand's pentadenticity allows the study of single site reactivity. A diverse set of exogenous monodentate ligands that spans the spectrochemical series can complete the octahedral coordination of the metal center. Both hs and ls Fe(II) complexes are isolated at RT, hinting at an intrinsic "spin ambivalence" of the $[Fe^{II}(PY5)(X)]^{n+}$ moiety. The exogenous axial ligand regulates many properties of the Fe(II) metal center, including its spin-state and redox potential. Ligation of PY5 generates an electron-deficient Fe(II) center that preferentially chelates anionic ligands while also favoring strong-field ligands. The solution chemistry with respect to

(27) Real, J. A.; Muñoz, M. C.; Faus, J.; Solans, X. *Inorg. Chem.* **1997**, *36*, 3008−3013.
(28) Roux, C.; Zarembowitch, J.; Itié, J.-P.; Polian, A.; Verdaguer, M. *Inorg. Chem.* **1996**, *35*, 574−580.
(29) Jonas, R. T.; Stack, T. D. P. *Inorg. Chem.* **1998**, *37*, 6615−6629.
(30) Covington, A. K.; Dickinson, T. *Physical Chemistry of Organic Solvent Systems*; Plenum Press: London, 1973; p 823.

basic ligands shows signs of being markedly different in aprotic versus protic media.

Experimental Section

Syntheses. All starting materials were purchased from Aldrich and used without further purification unless noted otherwise. $Fe^{II}(OTf)_2$ was synthesized according to a literature method.[31] Sodium hydride (60% oil dispersion) was washed with hexanes and dried in a vacuum. All solvents and gases were of analytical grade and were purified by literature methods.[32] CH_2Cl_2 was distilled from CaH_2 under N_2 and stored over 4 Å molecular sieves. MeCN was distilled from CaH_2 under N_2. MeOH was distilled from $Mg(OMe)_2$ under N_2 and stored in darkness over 4 Å molecular sieves. Anhydrous diethyl ether (ether) was stored over 4 Å molecular sieves. THF was distilled from K(s) under N_2. When air-free solutions were necessary, the solvents were degassed prior to use. All iron complexes for crystallographic analysis were synthesized and handled under a N_2 inert atmosphere using a MBraun Labmaster 130 glovebox or standard Schlenk-line techniques. Flash column chromatography was performed using silica gel 60, 230−400 mesh from EM Science (Gibbstown, NJ) using standard techniques.[33]

Instrumentation. ^{1}H NMR spectra were recorded on a Varian Gemini-400 (400 MHz) NMR spectrometer at RT, and chemical shifts are reported in ppm downfield from an internal TMS reference. Electronic spectra at RT were measured on either a Polytec X-dap fiber optics UV−vis diode array spectrophotometer or a Cary 50 Bio UV−vis spectrophotometer. Electrochemical measurements were recorded at 100 mV/s under N_2 at RT using a Bioanalytical Systems, Inc. CV-50W voltammetric analyzer, a platinum working electrode, a platinum wire auxiliary electrode, 0.1 M (n-Bu_4N)(ClO_4) supporting electrolyte, and a silver wire reference electrode, with all potentials referenced to the ferrocenium/ferrocene couple (in MeOH = +0.610 V vs SHE, in acetone +0.700 V vs SHE, ΔE = 0.079 V).[34] Solution magnetic moments were determined at RT by the Evans method.[17] Mass spectroscopy data (positive FAB, MALDI, and LSIMS) were collected by the Mass Spectrometry Facility, Department of Pharmaceutical Chemistry, University of California, San Francisco. The matrix for MALDI mass spectroscopy was α-cyano-4-hydroxycinnamic acid while that for LSIMS mass spectroscopy was either 3-nitrobenzoic acid or thioglycerol. Elemental analyses were performed by Desert Analytics (Tucson, AZ). Samples were heated under vacuum at 398 K for 5 h prior to elemental analysis with the exception of [Fe(PY5)-N_3](OTf), which was instead dried under vacuum for 1 h at RT prior to analysis.

Metal Complex Syntheses. The synthesis and characterization of 2,6-(bis-(bis-2-pyridyl)methoxymethane)pyridine (PY5), [Fe(PY5)-(MeOH)](OTf)$_2$, [Fe(PY5)(OMe)](OTf), [Fe(PY5)(MeCN)](OTf)$_2$,[14,16] and [Fe(PY5)(MeCN)](ClO_4)$_2$[15] have been described previously. The preparation of KOPh has been described previously.[35]

[Fe(PY5)(H_2O)](OTf)$_2$. Equimolar amounts of PY5 (0.077 g) and Fe(OTf)$_2$ (0.058 g) were dissolved in 10 mL of nondried 2-propanol under N_2. Addition of diethyl ether resulted in the precipitation of a yellow compound in nearly quantitative yield (0.123 g, 90%). Yellow/green crystals suitable for X-ray analysis were obtained from an 2-propanol/diethyl ether solution of the complex, [Fe(PY5)(H_2O)](OTf)$_2$. Absorption spectrum (2-propanol) λ_{max} (nm), ϵ (M^{-1} cm^{-1}): 355, 1580; 568, 20; 775, 20. Mass spectroscopy (LSIMS$^+$, M^+): *m*/*e* 698.0 (EM = 698.8 for [Fe-(PY5)(H_2O)](OTf)$^{1+}$). Cyclic voltammetry (acetone): +1.360 V versus SHE (ΔE = 0.180 V). Solution magnetic moment (acetone-d_6): $\mu_{eff} = 4.9\ \mu_B$. ^{1}H NMR (400 MHz, acetone-d_6) δ (ppm): −11.8, 14.5, 17.1, 41.9, 54.4, 58.0. Anal. Calcd for $C_{31}H_{27}N_5O_9F_6S_2Fe$: C, 43.93; H, 3.21; N, 8.26. Found: C, 44.02; H, 3.17; N, 8.18.

[Fe(PY5)(pyridine)](OTf)$_2$. Equimolar amounts of PY5 (0.034 g) and Fe(OTf)$_2$ (0.025 g) were dissolved in 2.0 mL of pyridine under N_2 to give a deep red/brown solution. Addition of diethyl ether resulted in the precipitation of a brown compound in moderate yield (0.048 g, 75%). Deep red prismatic crystals suitable for X-ray analysis were obtained from a pyridine/diethyl ether solution of the complex, [Fe(PY5)(pyridine)](OTf)$_2$·(pyridine). Absorption spectrum (pyridine) λ_{max} (nm), ϵ (M^{-1} cm^{-1}): 396, 4700; 440, 3000; 548, 190. Mass spectroscopy (LSIMS$^+$, M^+): *m*/*e* 680.0 (EM = 680.8 for [Fe(PY5)](OTf)$^{1+}$). Cyclic voltammetry (MeOH): +1.180 V vs SHE (ΔE = 0.100 V). Solution magnetic moment (acetone-d_6): $\mu_{eff} = 0\ \mu_B$. ^{1}H NMR (400 MHz, acetone-d_6): δ (ppm) 4.68 (6 H, s, C−OMe), 7.39 (4 H, d of d, J = 5.6 Hz, 3-Hpy-equatorial (eq)), 8.03 (4 H, t, J = 7.6 Hz, 4-Hpy-eq), 8.21 (1H, t, J = 4.4 Hz, 4-H of exogenous pyridine (py-ex)), 8.34 (1 H, t, J = 6.0 Hz, 4-Hpy-axial (ax)), 8.94 (2H, d, J = 6.7 Hz, 3-Hpy-ex), 9.69 (2 H, d, J = 6.0 Hz, 3-Hpy-ax), 10.05 (4 H, d, J = 7.2 Hz, 5-Hpy-eq), 10.89 (4 H, b, 6-Hpy-eq), 13.38 (2 H, b, 2-Hpy-ex). Anal. Calcd for $C_{36}H_{30}N_6O_8F_6S_2Fe$: C, 47.59; H, 3.33; N, 9.25. Found: C, 47.82; H, 3.19; N, 9.35.

[Fe(PY5)(OBz)](OTf). Equimolar amounts of [Fe(PY5)(MeOH)]-(OTf)$_2$ (0.036 g) and NaOBz (0.009 g) were dissolved in 4 mL of MeOH under N_2 to give a greenish-yellow solution. Addition of diethyl ether resulted in the precipitation of a greenish-yellow compound in nearly quantitative yield (0.032 g, 95%). Green prismatic crystals suitable for X-ray analysis were obtained from a slowly cooled MeOH solution of the complex, [Fe(PY5)(OBz)]-(OTf). Absorption spectrum (MeOH) λ_{max} (nm), ϵ (M^{-1} cm^{-1}): 330, 1630; 395, 1800. Mass spectroscopy (MALDI, M^+): *m*/*e* 681.1 (EM = 680.8 for [Fe(PY5)](OTf)). Cyclic voltammetry (MeOH): +1.025 V vs SHE (ΔE = 0.160 V). ^{1}H NMR (400 MHz, acetone-d_6): δ (ppm) −8.2, 5.11, 7.1, 7.9, 10.4, 18.3, 37.4, 51.5, 54.4. Anal. Calcd for $C_{37}H_{30}N_5O_7F_3SFe$·MeOH: C, 53.31; H, 4.11; N, 8.40. Found: C, 52.88; H, 3.61; N, 8.06.

[Fe(PY5)(N_3)](OTf). Nearly equimolar amounts of PY5 (0.042 g) and Fe(OTf)$_2$ (0.034 g) were dissolved in 2.0 mL of MeOH under N_2 to give a yellow solution. The addition of NaN_3 (0.0058 g) as a MeOH solution turns the solution orange. Upon standing, crystals precipitated in moderate yield (0.040 g, 65%). Absorption spectrum (MeOH) λ_{max} (nm), ϵ (M^{-1} cm^{-1}): 405, 2150; 810, 20. Mass spectroscopy (MALDI, M^+): *m*/*e* 681.1 (EM = 680.8 for [Fe(PY5)](OTf)). Cyclic voltammetry (MeOH): +0.740 V vs SHE (irrev). Solution magnetic moment (acetone-d_6): $\mu_{eff} = 4.7\ \mu_B$. ^{1}H NMR (400 MHz, acetone-d_6): δ (ppm) −9.8, 7.45, 19.35, 41.9, 51.9, 54.1. Anal. Calcd for $C_{30}H_{25}N_8O_5ClF_3SFe$: C, 49.90; H, 3.49; N, 15.52. Found: C, 50.03; H, 3.76; N, 15.22.

[Fe(PY5)(Cl)](OTf). Equimolar amounts of PY5 (0.050 g) and $FeCl_2$ (0.013 g) were dissolved in 5 mL of MeOH under N_2 to give a deep orange solution. Addition of 1 equiv of Ag(OTf) (0.027 g) resulted in a deep yellow solution and the precipitation of AgCl. After filtration of the solution, addition of diethyl ether resulted in the precipitation of a bright yellow compound in nearly quantitative

(31) Haynes, J. S.; Sams, J. R.; Thompson, R. C. *Can. J. Chem.* **1981**, *59*, 669−678.
(32) Perrin, D. D.; Armarego, W. L. F. *Purification of Laboratory Chemicals*, 1st ed.; Pergamon Press: New York, 1988.
(33) Still, W. C.; Kahn, M.; Mitra, A. *J. Org. Chem.* **1978**, *43*, 2923−2925.
(34) Zuman, P.; Meites, L. *Electrochemical Data*; John Wiley & Sons: New York, 1974; Vol. A.
(35) Krafft, T. E.; Hejna, C. I.; Smith, J. S. *Inorg. Chem.* **1990**, *29*, 2682−2688.

yield (0.078 g, 95%). Yellow prismatic crystals suitable for X-ray analysis were obtained from a MeOH/diethyl ether solution of the complex, [Fe(PY5)(Cl)](OTf)·(MeOH). Absorption spectrum (MeOH) λ_{max} (nm), ϵ (M^{-1} cm^{-1}): 330, 1590; 390, 1930; 860, 15. Mass spectroscopy (LSIMS$^+$, M^+): *m*/*e* 567.5 (EM = 567.3 for [Fe(PY5)(Cl)]$^{1+}$). Cyclic voltammetry (MeOH): +0.990 V vs SHE (ΔE = 0.090 V). Solution magnetic moment (acetone-d_6): μ_{eff} = 5.1 μ_B. ^{1}H NMR (400 MHz, acetone-d_6): δ (ppm) −11.2, 7.9, 18.3, 42.6, 50.2, 64.1. Anal. Calcd for $C_{30}H_{25}N_5O_5ClF_3SFe$: C, 50.33; H, 3.52; N, 9.79. Found: C, 49.95; H, 3.78; N, 9.57.

[Fe(PY5)(CN)](OTf). Addition of 1 equiv of KCN (0.005 g) to a 10 mL MeOH solution of [Fe(PY5)(MeOH)](OTf)$_2$ (0.053 g) under N_2 resulted in the deep red ferrous cyanide species [Fe(PY5)(CN)](OTf) at RT. A red crystalline solid was isolated after addition of diethyl ether in nearly quantitative yield (0.042 g, 90%). Deep red prismatic crystals suitable for X-ray analysis were obtained from a MeOH/diethyl ether solution of the complex, [Fe(PY5)(CN)](OTf)·(MeOH). Absorption spectrum (MeOH) λ_{max} (nm), ϵ (M^{-1} cm^{-1}): 372, 6700; 439, 8100. Mass spectroscopy (LSIMS$^+$, M^+): *m*/*e* 557.1 (EM = 557.4 for [Fe(PY5)(CN)]$^{1+}$). Cyclic voltammetry (MeOH): +0.920 V vs SHE (ΔE = 0.085 V). Solution magnetic moment (acetone-d_6): μ_{eff} = 0 μ_B. ^{1}H NMR (400 MHz, acetone-d_6): δ (ppm) 4.03 (6 H, s, C−OMe), 7.46 (4 H, d of d, J = 5.5 Hz, 3-Hpy-equatorial (eq)), 7.93 (4 H, t, J = 6.8 Hz, 4-Hpy-eq), 8.01 (4 H, d, J = 4.2 Hz, 5-Hpy-eq), 8.32 (3 H, m, py-axial), 10.11 (4 H, d, J = 5.2 Hz, 6-Hpy-eq). Anal. Calcd for $C_{31}H_{25}N_6O_5F_3SFe$·MeOH: C, 50.42; H, 3.96; N, 11.38. Found: C, 49.23; H, 3.40; N, 10.39.

[Fe(PY5)(OPh)](OTf). Equimolar amounts of [Fe(PY5)(MeOH)](OTf)$_2$ (0.050 g) and KOPh (0.010 g) were dissolved in 10 mL of acetone under N_2 to give an orange solution. Addition of diethyl ether resulted in the precipitation of an orange-red powder in moderate yield (0.027 g, 60%). Absorption spectrum (MeOH) λ_{max} (nm), ϵ (M^{-1} cm^{-1}): 355, 1660; 430, 1530. Mass spectroscopy (MALDI, M^+): *m*/*e* 681.1 (EM = 680.8 for [Fe(PY5)](OTf)). Cyclic voltammetry (acetone): +1.070 V vs SHE (ΔE = 0.090 V). Solution magnetic moment (acetone-d_6): μ_{eff} = 4.9 μ_B. ^{1}H NMR (400 MHz, acetone-d_6): δ (ppm) −5.8, 6.7, 19.6, 38.8, 43.1, 47.1, 51.4, 54.5, 56.2.

Equilibrium Constant Measurements. The relative binding affinities of various exogenous ligands were determined in MeOH by spectrophotometric titrations. The exogenous ligand titrants were added either as neat solutions (MeCN, pyridine) or as MeOH solutions (Et_4NCl, NaN_3) of the added species. MeCN and pyridine were added to ~0.5 mM solutions of [Fe(PY5)(MeOH)](OTf)$_2$. The binding affinities of anionic ligands relative to MeOH are too large to directly assess by optical spectroscopy. Instead, the binding affinities of anionic ligands were measured relative to that of pyridine. These titrations were performed in a mixed pyridine/MeOH solution (25% pyridine by volume) to ensure >99% conversion of [Fe(PY5)(MeOH)]$^{2+}$ to [Fe(PY5)(pyridine)]$^{2+}$. Solutions of Et_4NCl and NaN_3 were titrated to ~0.5 mM [Fe(PY5)(pyridine)](OTf)$_2$. Because of solubility issues, an inverse titration was performed to measure the relative binding affinity of OBz^-, with pyridine added to a 0.2 mM MeOH solution of [Fe(PY5)(OBz)](OTf). For each titration, at least five independent spectra covering the 350−500 nm wavelength range were collected. Factor analysis in SPECFIT showed that only two colored species were present above the limit of detection. The titration data were sufficiently modeled with a single equilibrium expression (eq 1). The component spectra of the two pure colored species and the equilibrium constant were refined to minimize the residual between the observed absorbance at each wavelength and that calculated from the model for all independent spectra.

X-ray Crystallography. ORTEP representations with a detailed numbering scheme and complete tables of positional parameters, bond lengths, bond angles, and anisotropic thermal factors for the described crystal structures are located in the Supporting Information.

General Methods. For each of the X-ray crystal structures presented, the data set was collected at low temperature <200 K under a N_2 stream. A suitably sized crystal was mounted in paratone oil on a glass fiber and placed in a cold stream of N_2 on an Enraf-Nonius CAD-4 or a Siemens CCD diffractometer with graphite monochromated Mo Kα radiation (λ = 0.710 73 Å). Structural and refinement data for the four high-spin and two low-spin ferrous complexes are summarized in Tables 4 and 5, respectively. The data were corrected for Lorentz and polarization effects. The structures were solved by direct methods and expanded using Fourier techniques. All non-hydrogen atoms were refined anisotropically, unless noted. Hydrogen atoms were located by difference Fourier maps but included at idealized position 0.95 Å from their parent atoms for the final refinement. Isotropic thermal parameters 1.2 times the parent atoms were assumed. Unless otherwise noted, the remaining significant peaks on the final difference Fourier maps were located near the triflate anion(s). Neutral atom scattering factors were taken from Cromer and Waber.[36] Anomalous dispersion effects were included in F_{calcd};[37] the values for $\Delta f'$ and $\Delta f''$ were those of Creagh and McAuley.[38] The values for the mass attenuation coefficients are those of Creagh and Hubbell.[39] All calculations were performed using the teXsan crystallographic software package of Molecular Structure Corporation. Specific details for each of the crystal structures are available.[18]

Acknowledgment. We are grateful to the National Institutes of Health (Grant GM50730) and the Stanford Graduate Fellowship Fund (C.R.G.) for financial support of this work.

(36) Cromer, D. T.; Waber, J. T. *International Tables for X-ray Crystallography*; Kynoch: Birmingham, 1974; Vol. IV.
(37) Ibers, J. A.; Hamilton, W. C. *Acta Crystallogr.* **1964**, *17*, 781−782.
(38) Creagh, D. C.; McAuley, W. J. In *International Tables for Crystallography*; Wilson, A. J. C., Ed.; Kluwer Academic Publishers: Boston, 1992; Vol. C.; p 219−222, Table 4.2.6.8.
(39) Creagh, D. C.; Hubbell, J. H. In *International Tables for Crystallography*; Wilson, A. J. C., Ed.; Kluwer Academic Publishers: Boston, 1992; Vol. C.; p 200−206, Table 4.2.4.3.
(40) Orville, A. M.; Lipscomb, J. D.; Ohlendorf, D. H. *Biochemistry* **1997**, *36*, 10052−10066.
(41) Ohlendorf, D. H.; Orville, A. M.; Lipscomb, J. D. *J. Mol. Biol.* **1994**, *244*, 586−608.
(42) Senda, T.; Sugiyama, K.; Narita, H.; Yamamoto, T.; Kimbara, K.; Fukuda, M.; Sato, M.; Yano, K.; Mitsui, Y. *J. Mol. Biol.* **1996**, *255*, 735−752.
(43) Han, S.; Eltis, L. D.; Timmis, K. N.; Muchmore, S. W.; Bolin, J. T. *Science* **1995**, *270*, 976−980.
(44) Minor, W.; Steczko, J.; Stec, B.; Otwinowski, Z.; Bolin, J. T.; Walter, R.; Axelrod, B. *Biochemistry* **1996**, *35*, 10687−10701.
(45) Boyington, J. C.; Gaffney, B. J.; Amzel, L. M. *Science* **1993**, *260*, 1482−1486.
(46) Gillmor, S. A.; Villaseñor, A.; Fletterick, R.; Sigal, E.; Browner, M. F. *Nat. Struct. Biol.* **1997**, *4*, 1003−1009.
(47) Erlandsen, H.; Fusetti, F.; Martinez, A.; Hough, E.; Flatmark, T.; Stevens, R. C. *Nat. Struct. Biol.* **1997**, *4*, 995−1000.
(48) Zhang, Z.; Ren, J.; Stammers, D. K.; Baldwin, J. E.; Harlos, K.; Schofield, C. J. *Nat. Struct. Biol.* **2000**, *7*, 127−133.
(49) Kreisberg-Zakarin, R.; Borovok, I.; Yanko, M.; Frolow, F.; Aharonowitz, Y.; Cohen, G. *Biophys. Chem.* **2000**, *86*, 109−118.
(50) Sugio, S.; Hiraoka, B. Y.; Yamakura, F. *Eur. J. Biochem.* **2000**, *267*, 3487−3495.
(51) Yeh, A. P.; Hu, Y.; Jenney, F. E., Jr.; Adams, M. W. W.; Rees, D. C. *Biochemistry* **2000**, *39*, 2499−2508.

Supporting Information Available: Structure reports for [Fe(PY5)(H_2O)]($OTf)_2$, [Fe(PY5)(OBz)](OTf), [Fe(PY5)(Cl)](OTf), [Fe(PY5)(pyridine)]($OTf)_2$, and [Fe(PY5)(CN)](OTf); comparison of the anticipated $[Fe(PY5)(pyridine)]^{2+}$ spectrum to an independently obtained spectrum; structural overlay RMS errors for the ferrous complex six-coordinate coordination cores. This material is available free of charge via the Internet at http://pubs.acs.org.

IC025616Z